# Numerical modeling of salt and gypsum dissolution: test case and comparison

Farid Laouafa, Jianwei Guo, Michel Quintard

# Numerical modeling of salt and gypsum dissolution: Test case and comparison

*Farid Laouafa[1]*, Jianwei Guo[2], Michel Quintard[3]*

*[1]Institut National de l'Environnement Industriel et des Risques- INERIS (France), Verneuil-en-Halate, F-60550, France; [2]School of Mechanics and Engineering, Southwest Jiaotong University, 61003 Chengdu, China; [3]Université de Toulouse; INPT, UPS, IMFT (Institut de Mécanique des Fluides de Toulouse), Allée Camille Soula, F-31400 Toulouse, France and CNRS, IMFT, F-31400 Toulouse, France*

** farid.laouafa@ineris.fr*

ABSTRACT: This paper deals with the dissolution of certain soluble rocks such as salt and gypsum, and the geomechanical consequences like subsidence, sinkholes, underground collapses. It focuses on salt and gypsum, although the developed method can be used for any soluble rock. In this paper, a large-scale Diffuse Interface Model (DIM) is used to describe the evolution of a salt cavity formed by dissolution. The method is based upon the assumption of a pseudo-component dissolving with a thermodynamic equilibrium boundary condition. The purpose of this article is to provide a review the method we have developed and more specifically to present its possibilities. The problems considered are isothermal even if the temperature field could be easily integrated into the global physical problem. The potential of the proposed methodology is illustrated on one meso-scale (in-situ) configuration corresponding to salt cavity dissolution. Comparison between in-situ experiment data and numerical modeling shows the method is a good prediction tool. A final boundary value problem is also studied in which salt is replaced by gypsum to show the applicability of the proposed methodology to analyze rocks with different solubility.

## 1 Introduction

Dissolution of porous media or solids is a major concern in many industrial fields. Many sinkholes, soil or rock collapses are the consequences of the dissolution of underground evaporite such as gypsum. Rock dissolution creates underground cavities of different shapes and sizes, with a potential risk of collapse as illustrated in Figure 1. Thus, in many applications, modeling such liquid/solid dissolution problems is therefore of paramount importance.

Cavity dissolution is a mechanism of great significance in the onset of sinkholes. To be able to predict the occurrence of critical subsidence or sinkhole onset, it is necessary to have a better knowledge of the dissolution process. Indeed, even if we know the critical sizes of a cavity leading to the appearance of a sinkhole, one rarely knows the time needed to reach it. A transient analysis of the dissolution answers this question.

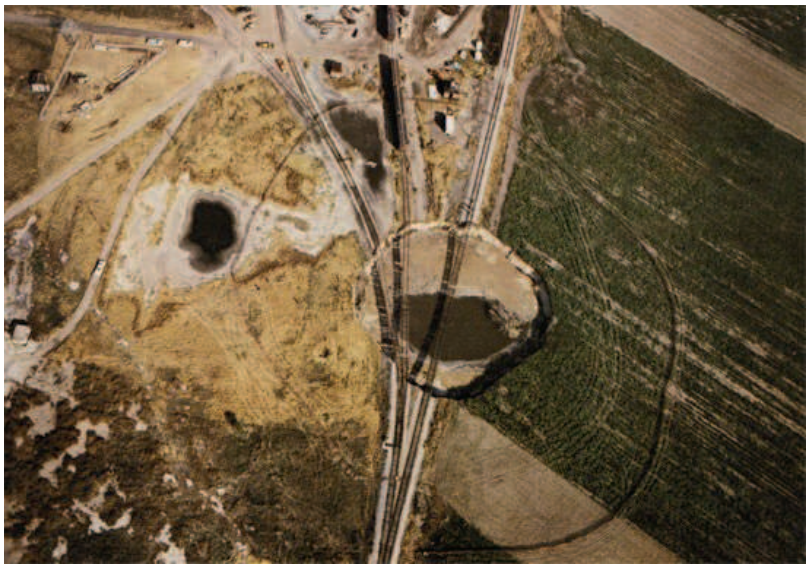

Figure 1: Land Subsidence (sinkhole) in Central Kansas related to Salt dissolution.

Using dissolution modeling also enables the optimization of the industrial dissolution process. This optimization can relate, for example, to the intensity of the input flow, the temperature of the injected fluid, the degree of saturation of the inlet fluid, the location of the injection wells, etc. Rock dissolution is undoubtedly a multi-scale and multiphysics problem raising several questions. One concerns an accurate description of solid-liquid interface recession at the macro-scale level. In order to reach this goal, it is essential to have a precise mathematical formalization of physicochemical and transport mechanisms at the micro scale level. The second concerns the applicability to large spatial scale. Finally, strong coupling with other physical processes, in particular geomechanical behavior, must be considered.

In practice, local dissolution rate models are often assumed at the macroscopic level. Empirical models, averaged models, based on laboratory tests or in-situ observations are often used to describe dissolution in an average sense. Accurate solving of real dissolution problems has shown that entrance and heterogeneity effects, or natural convection, and that these simple averaged models are not suitable. This paper, discusses these different questions, based on theoretical and numerical analysis of several examples.

Our analysis starts at the scale of the dissolving surface and the choice of the surface dissolution kinetics. This has been the subject of many studies for various dissolving materials. Most generally, the surface reaction rate, $R$, which appears in the boundary condition for the micro-scale dissolution problem for limestone, calcite, gypsum, or salt follows a general form expressed as (Jeschke et al. 2001; Jeschke and Dreybrodt, 2002):

$$R = k\left(1 - \frac{C}{C_{eq}}\right)^{n}$$

Where $k$ is the surface reaction rate coefficient, $C$ is the mass concentration of the dissolved species at the surface, and $C_{eq}$ the equilibrium concentration (solubility). If at the surface Damköhler number is very large, for instance through a very large value of $k$, this boundary condition tends to the classical equilibrium condition expressed by $C = C_{eq}$ at the solid surface. This latter condition is often used for salt dissolution, for instance. Assuming such an approximation is valid, we restrict our discussion to two different ways for modeling the dissolution problem: (i) a direct treatment of the evolution of the fluid-solid interface using an ALE (Arbitrary Lagrangian-Eulerian) method (Donea et al. 1982), (ii) the use of a Diffuse Interface Model (*DIM*) to smooth the interface with continuous quantities (Anderson et al. 1998, Collins et al. 1985, Luo et al. 2012), like the liquid phase volume fraction, species mass fractions, etc.

Given this presentation of the research background about dissolution models, the objective of this paper is set as a discussion about the development of large-scale (e.g. tenths of meters) dissolution models representative of situations encountered in geotechnical or geomechanical fields. In terms of soluble bedrock, salt (NaCl) and gypsum ($CaSO_4 \cdot 2H_2O$) are considered. Concerning carbonate rocks, which spread the most widely worldwide, the methodology may be extended easily while the quantitative conclusions presented in this paper are of course specific to the cases under consideration (i.e., salt and gypsum).

While the quantitative conclusions presented in this paper are of course specific to the salt case, the methodology may be reproduced for gypsum, limestone, or carbonate dissolution problems. The main objective of Section 2 is to present briefly the physical and mathematical base of the two dissolution models. In this section, the diffuse interface model is deduced with the help of a volume averaging theory. We formulate the dissolution problem at the pore scale and then deduce the macroscopic effective parameters by using an upscaling technique. The approach is depicted in Figure 2.

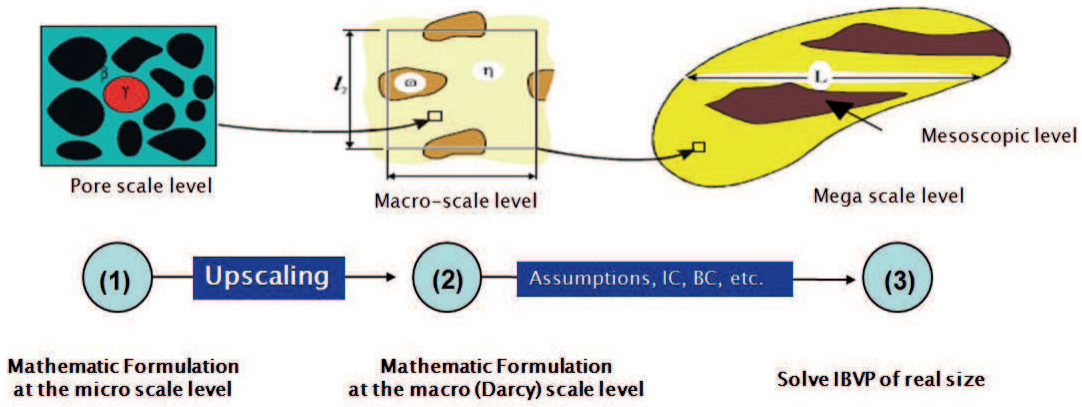


Figure 2: From micro-scale (pore scale level) to large-scale levels (caverns scale). Macro scale level is the Darcy-scale level (classical sample scale)

Next, we show that our model can capture the instability pattern such as roughness onset during the dissolution of a porous medium, which is known to be a very difficult numerical problem. Therefore, it can be used as a diffuse interface model to simulate dissolution problems instead of explicit tracking of the dissolution interface (such as in ALE frameworks) which faces in this case huge numerical difficulties.

For most transient problems, we may have very high concentration gradients and, therefore, neglecting strong density gradients may bring inaccuracy to the prediction of dissolution and fluid flow. This may be the case with salt formations since the solubility of salt is around 360 g/l in comparison with that of gypsum which is about 2.6 g/l. Consequently, the density gradient should be considered in general for an accurate analysis, and, in this paper, the Darcy-scale diffuse interface model (DIM) includes density driven flows is deduced from the original liquid/solid dissolution in the case of a binary other systems (following Golfier et al. (2002), Guo et al. (2015)). The model is applied to several cases and a final comparison of the same dissolution boundary value problems involving the same boundary conditions, is performed using salt or gypsum as soluble rocks. Results show that not only the size of the cavity changes but also the shape. We finally conclude by a discussion concerning the dissolution rate.

## 2 Dissolution models

Two types of dissolution models are considered. The original dissolution problem corresponding to a sharp liquid/solid interface is illustrated in Figure 3. The solid/liquid interface is described mathematically by a surface at which the liquid concentration is equal to an equilibrium concentration. If we introduce a scalar phase indicator, such as porosity $\varepsilon_\beta$ (volume fraction of the β-phase in this case), it has a value of 1 in the liquid and zero elsewhere, with a jump at the interface as illustrated in Figure 3.

Solving such a dissolution mathematical problem requires a special front tracking numerical technique, which is often computationally time consuming. Alternative models do not require an explicit treatment of the moving interface. Instead, partial differential equations are written for continuous variables, such as $\varepsilon_\beta$ and the *mass fraction* $\omega_{A\beta}$ (mass fraction of species A in the β-phase), which lead to a diffuse interface as illustrated in Figure 3. We will present below the two formulations.

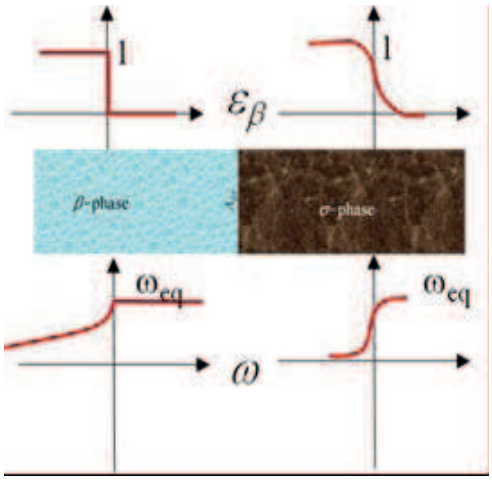


Figure 3: Original dissolution model (sharp interface on the left) and Diffuse Interface Model (on the right).

The original solid/liquid dissolution problem can be described by classical convective-diffusive mass balance and Navier-Stokes (momentum) equations, etc. To express the DIM model, we start from these original solid/liquid equations to generate averaged or Darcy-scale equations involving effective coefficients (Luo, et al. 2012, Guo et al. 2015), and taking into account the density as a function of concentration. In the first subsection, the original model for the dissolution problem is introduced. In the second subsection, we briefly introduce the upscaling method leading to the “Darcy-scale” equations which are used as the basis for the DIM formulation.

## *2.1 The original multiphase model*

Let us consider a binary liquid phase β containing chemical species A and B, and a solid phase σ containing only chemical species A. We neglect the effect of temperature, even if it can be easily integrated. The general formulation integrates gravity and thus density gradients into the corresponding equations.

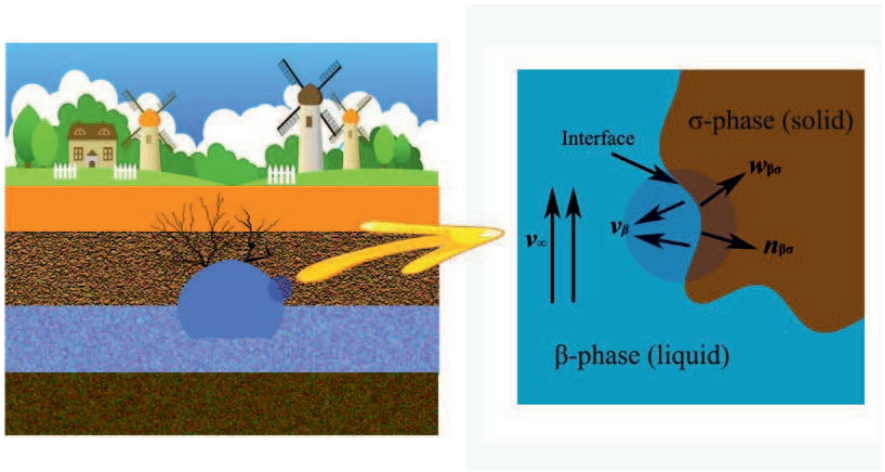


Figure 4: Large-scale (left) and near interface scale(right).

In Figure 4 (right), $\boldsymbol{v}_{\infty}, \boldsymbol{v}_{\beta}, \boldsymbol{w}_{\beta\sigma}, \boldsymbol{n}_{\beta\sigma}$ represent the velocity of the fluid far away from the interface, the velocity of the phase β near the interface, the recession rate, and the normal to the interface, respectively. In the following, bold letters indicate either vector or tensor variables. The four equations bellows are formulated inside the fluid domain, while the others at the interface level.

The total mass balance equation for the β-phase is

$$\frac{\partial \rho_{\beta}}{\partial t} + \nabla \cdot \left( \rho_{\beta} \boldsymbol{v}_{\beta} \right) = 0 \tag{1}$$

The mass balance equations for any species A in the β-phase is written as,

$$\frac{\partial \left( \rho_{\beta} \omega_{A\beta} \right)}{\partial t} + \nabla \cdot \left( \rho_{\beta} \omega_{A\beta} \boldsymbol{v}_{A\beta} \right) = 0 \tag{2}$$

The general mass balance equation for a moving σ-phase is written as

$$\frac{\partial \rho_{\sigma}}{\partial t} + \nabla \cdot \left( \rho_{\sigma} \boldsymbol{v}_{\sigma} \right) = 0 \tag{3}$$

In the case of the fluid, we will use the Navier-Stokes equations for the momentum balance, considering gravity fields and fluid pressure., i.e.,

$$\rho_{\beta} \left( \frac{\partial \boldsymbol{v}_{\beta}}{\partial t} + \boldsymbol{v}_{\beta} \cdot \nabla \boldsymbol{v}_{\beta} \right) = \rho_{\beta} \ \mathbf{g} - \nabla p_{\beta} + \mu_{\beta} \ \nabla^2 \boldsymbol{v}_{\beta} \tag{4}$$

where $\boldsymbol{v}_{\beta}$ represents the velocity of the β-phase, $\nabla p_{\beta}$ the pressure gradient in the β-phase, $\mu_{\beta}$ the dynamic viscosity of the β-phase and **g** the gravity vector. At the β-σ interface $A_{\beta\sigma}$, the chemical potentials $\psi$ for each species should be equal for the distinct phases. In this case and for the special binary case under investigation, we have the following equality at a given pressure *p* and temperature *T*:

$$\psi_{A\beta} \left( \omega_{A\beta}, p, T \right) = \psi_{A\sigma} \left( \omega_{A\sigma}, p, T \right) \quad \text{at} \quad A_{\beta\sigma} \tag{5}$$

where $\omega_{A\sigma}$ is equal to 1. It must be emphasized that in the complete binary case, i.e., when $\omega_{A\sigma}$ is not equal to 1, there is also a relation similar to the above equation for the other components.

This results in the classical equilibrium condition, i.e.,

$$\omega_{A\beta} = \omega_{eq} \qquad \text{at} \qquad A_{\beta\sigma} \tag{6}$$

where $\omega_{eq}$ is the equilibrium concentration for species A.

We deduce from the mass balances for species A and B the following relations at the $\beta-\sigma$ interface:

$$\begin{cases}\rho_\beta \omega_{A\beta}\left(\boldsymbol{v}_{A\beta}-\boldsymbol{w}\right)\cdot\boldsymbol{n}_{\beta\sigma}=\rho_\sigma \omega_{A\sigma}\left(\boldsymbol{v}_{A\sigma}-\boldsymbol{w}\right)\cdot\boldsymbol{n}_{\beta\sigma} \text{ at } A_{\beta\sigma}\\ \rho_\beta \omega_{B\beta}\left(\boldsymbol{v}_{B\beta}-\boldsymbol{w}\right)\cdot\boldsymbol{n}_{\beta\sigma}=\rho_\sigma \omega_{B\sigma}\left(\boldsymbol{v}_{B\sigma}-\boldsymbol{w}\right)\cdot\boldsymbol{n}_{\beta\sigma} \text{ at } A_{\beta\sigma}\end{cases} \tag{7}$$

where $\boldsymbol{w}$ represents the velocity of the interface with $\boldsymbol{n}_{\beta\sigma}$ the interface normal vector. One of these equations can be alternatively replaced by the sum, or total mass balance requirement at the $\beta-\sigma$ interface

$$\rho_\beta\left(\boldsymbol{v}_\beta-\boldsymbol{w}\right)\cdot\boldsymbol{n}_{\beta\sigma}=\rho_\sigma\left(\boldsymbol{v}_\sigma-\boldsymbol{w}\right)\cdot\boldsymbol{n}_{\beta\sigma} \text{ at } A_{\beta\sigma} \tag{8}$$

with the definition $\boldsymbol{v}_\sigma=\boldsymbol{v}_{A\sigma}$. From the above equations and using a theory of diffusion (Taylor and Krishna, 1993), we have

$$\rho_\beta \omega_{A\beta}\boldsymbol{v}_{A\beta}=\rho_\beta \omega_{A\beta}\boldsymbol{v}_\beta-\rho_\beta D_{A\beta}\nabla\omega_{A\beta} \tag{9}$$

Then,

$$\begin{aligned}&\rho_\beta \omega_{A\beta}\left(\boldsymbol{v}_{A\beta}-\boldsymbol{w}\right)\cdot\boldsymbol{n}_{\beta\sigma}=\\ &\boldsymbol{n}_{\beta\sigma}\cdot\left(\rho_\beta \omega_{A\beta}\left(\boldsymbol{v}_\beta-\boldsymbol{w}\right)-\rho_\beta D_{A\beta}\nabla\omega_{A\beta}\right) \text{ at } A_{\beta\sigma}\end{aligned} \tag{10}$$

The mass balance for species A, can then be expressed as follows:

$$\frac{\partial\left(\rho_\beta \omega_{A\beta}\right)}{\partial t}+\nabla\cdot\left(\rho_\beta \omega_{A\beta}\boldsymbol{v}_\beta\right)=\nabla\cdot\left(\rho_\beta D_{A\beta}\nabla\omega_{A\beta}\right) \tag{11}$$

The whole balance equations presented above are sufficient to solve the physical problem, provided that the overall surrounding boundary conditions are also given. After some equation transformations, we have the two following expressions:

$$\boldsymbol{n}_{\beta\sigma}\cdot\boldsymbol{v}_\beta=\boldsymbol{n}_{\beta\sigma}\cdot\left(\boldsymbol{v}_\sigma+\frac{\rho_\beta \quad \rho_\sigma}{\rho_\sigma(1 \quad \omega_\beta)}D_{A\beta}\nabla \quad _{A\beta}\right) \text{ at } A_{\beta\sigma} \tag{12}$$

$$\boldsymbol{n}_{\beta\sigma}\cdot\boldsymbol{w}=\boldsymbol{n}_{\beta\sigma}\cdot\left(\boldsymbol{v}_\sigma+\frac{\rho_\beta}{\rho_\sigma(1-\omega_{A\beta})}D_{A\beta}\nabla\omega_{A\beta}\right) \text{at } A_{\beta\sigma} \tag{13}$$

where $D_{A\beta}$ represents the diffusion coefficient.

This last equation relates explicitly the recession velocity to the transport flux and can be used to compute the interface movement in ALE. The dissolution problem is completed with the set of equations to describe the boundary and initial conditions of the fluid domain.

The simulation of the dissolution process has been implemented using ALE in COMSOL®. Because of the complex movement of the interface, frequent re-gridding is required and the resolution near the interface cannot be very fine or else creates rapid unacceptable distortion of the mesh. Some of the numerical difficulties associated with very sharp fronts can be circumvented by using a Diffuse Interface Method. Contrary to “sharp methods”, a diffuse interface method considers the interface as a smooth transition layer where the quantities vary continuously. The whole domain constituted by the two phases is considered to be a continuous medium without any singularities nor a strict distinction of solid or liquid (see Figure 3).

Neglecting the density variation, Golfier et al. (2002) studied one example of dissolution diffuse interface model. It corresponds to a porous medium non-equilibrium dissolution model involving a mass exchange coefficient $\alpha$ . It has the ability to be very close, with a proper choice of the exchange term (i.e., $\alpha$ ) to the local equilibrium solution, which is equivalent to the original dissolution problem.

Golfier et al. (2002) work may be extended, as summarized in the following subsection, to incorporate the effect of density variation (Luo et al. 2012, Luo et al. 2015).

## *2.2 Darcy non-equilibrium model*

In the following analysis, the σ-phase is supposed immobile, i.e., $\boldsymbol{v}_\sigma = 0$ .

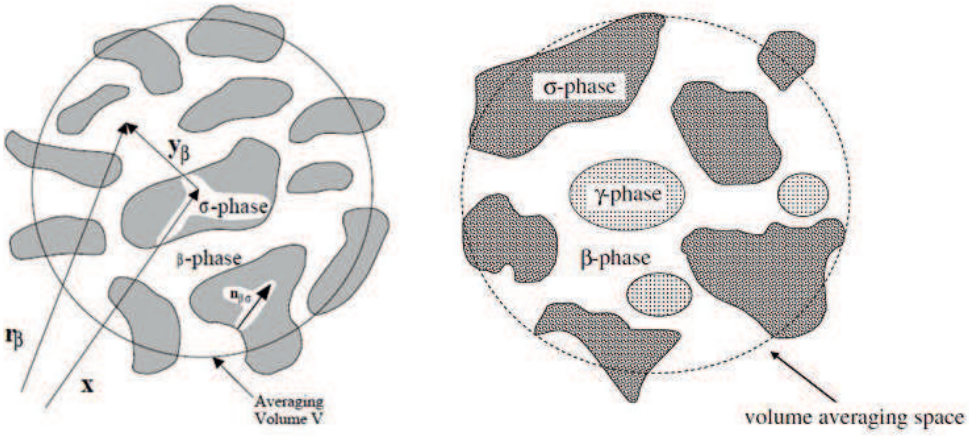


Figure 5: Averaging volume at pore scale level and material point position vector (left) and 3-phases model (the third phase may be insoluble species for instance) (right).

The volume averaging theory (Quintard and Whitaker 1994, Whittaker 1999) will be used to upscale the balance equations formulated at the pore scale (Figure 5). We define the intrinsic average of the mass fraction as

$$\Omega_{A\beta} = \left\langle \omega_{A\beta} \right\rangle^{\beta} = \varepsilon_\beta^{-1} \left\langle \omega_{A\beta} \right\rangle = \frac{1}{V_\beta} \int_{V_\beta} \omega_{A\beta}(\boldsymbol{r})\, dV \tag{14}$$

and the superficial average of the velocity as

$$\boldsymbol{V}_\beta = \left\langle \boldsymbol{v}_\beta \right\rangle = \varepsilon_\beta \left\langle \boldsymbol{v}_\beta \right\rangle^\beta = \frac{1}{V}\int_{V_\beta} \boldsymbol{v}_\beta \left(\boldsymbol{r}\right) dV \tag{15}$$

where $\boldsymbol{V}_\beta$ is the filtration velocity and $\mathbf{U}_\beta = \left\langle \boldsymbol{v}_\beta \right\rangle^\beta$ is the β-phase intrinsic average velocity. The averaged form of balance equation of species A can be expressed as:

$$\frac{\partial \left\langle \rho_\beta \omega_{A\beta} \right\rangle}{\partial t} + \nabla \cdot \left\langle \rho_\beta \omega_{A\beta} \boldsymbol{v}_{A\beta} \right\rangle = -\frac{1}{V}\int_{A_{\beta\sigma}} \boldsymbol{n}_{\beta\sigma} \cdot \rho_\beta \omega_{A\beta} \left(\boldsymbol{v}_{A\beta} - \boldsymbol{w}\right) \tag{16}$$

The above equation can then be transformed as:

$$\underbrace{\frac{\partial \left\langle \rho_\beta \omega_{A\beta} \right\rangle}{\partial t}}_{(\boldsymbol{a})} + \underbrace{\nabla \cdot \left\langle \rho_\beta \omega_{A\beta} \boldsymbol{v}_\beta \right\rangle}_{(\boldsymbol{b})} = \underbrace{\nabla \cdot \left\langle \rho_\beta D_{A\beta} \nabla \omega_{A\beta} \right\rangle}_{(\boldsymbol{c})} \underbrace{-\frac{1}{V}\int_{A_{\beta\sigma}} \boldsymbol{n}_{\beta\sigma} \cdot \rho_\beta \omega_{A\beta} \left(\boldsymbol{v}_{A\beta} - \boldsymbol{w}\right) dA}_{(\boldsymbol{d})} \tag{17}$$

The different terms (a), (b), (c) and (d) express:*(a) accumulation, (b)convection, (c) diffusion, and (d) the phase exchange* terms, respectively. After several assumptions and some mathematical treatment of the different equations we have the following control equations for the diffuse interface model (DIM) (Luo et al. 2012):

$$\varepsilon_\beta \rho_\beta^* \frac{\partial \Omega_{A\beta}}{\partial t} + \rho_\beta^* \boldsymbol{V}_\beta \cdot \nabla \Omega_{A\beta} = \nabla \cdot \left(\varepsilon_\beta \rho_\beta^* \boldsymbol{D}_{A\beta}^* . \nabla \Omega_{A\beta}\right) + \quad \rho_\beta^* \alpha \left(1 - \Omega_{A\beta}\right)\left(\omega_{eq} - \Omega_{A\beta}\right) \tag{18}$$

$$\frac{\partial \varepsilon_\beta \rho_\beta^*}{\partial t} + \nabla \cdot \left(\rho_\beta^* \boldsymbol{V}_\beta\right) = \rho_\beta^* \alpha \left(\omega_{eq} - \Omega_{A\beta}\right) \tag{19}$$

and

$$-\rho_\sigma \frac{\partial \varepsilon_\sigma}{\partial t} = \rho_\sigma \frac{\partial \varepsilon_\beta}{\partial t} = \rho_\beta^* \alpha \left(\omega_{eq} - \Omega_{A\beta}\right) \tag{20}$$

where $\boldsymbol{D}_{A\beta}^*$ is the macroscopic diffusion/dispersion coefficient, $\rho_\beta^*$ is such that $\left\langle \rho_\beta \omega_{A\beta} \right\rangle = \varepsilon_\beta \rho_\beta^* \Omega_{A\beta}$ and $\alpha$ is the exchange term between the two phases. The macroscopic diffusion/dispersion coefficient and the exchange term are obtained by solving “closure problems” provided by the theory over different types of unit cells representative of the porous medium, as illustrated Figure 6.

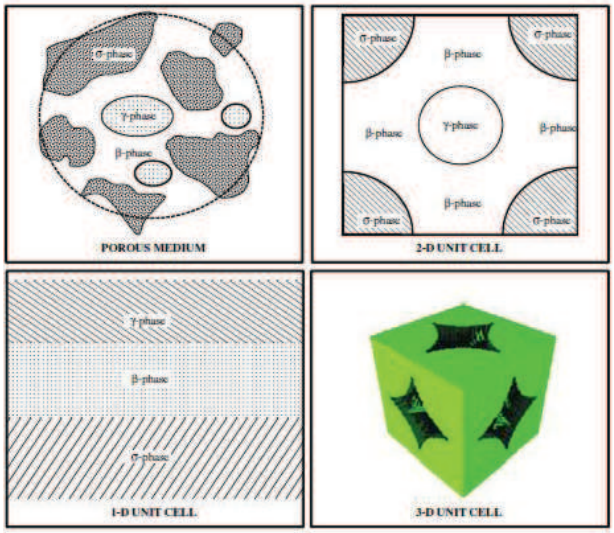


Figure 6: Examples of 1D, 2D and 3D unit cells (after Courtelieris and Delgado 2012).

Closure problems correspond to an approximate solution of the coupled problem: averaged variables/deviations. The approximate solution takes often the form of a mapping such

$$\tilde{\omega}_{A\beta} = \boldsymbol{b}_\beta \cdot \nabla \Omega_{A\beta} + s_\beta \left( \omega_{eq} - \Omega_{A\beta} \right) \tag{21}$$

where $\tilde{\omega}_{A\beta}$ is the concentration deviation and $\boldsymbol{b}_\beta$ and $s_\beta$ are the two closure variables. Solving two boundary value closure problems for $\boldsymbol{b}_\beta$ and $s_\beta$ allows us to express the macroscopic effective values according to the characteristics at the microscopic scale (pore scale). In other words, the physical properties at the macroscopic level are not “phenomenological” values but built on the basis of physical properties observed-defined at the microscopic scale.

In our case, we obtain the effective macroscopic diffusion tensor $\boldsymbol{D}^*_{A\beta}$, the macroscopic effective exchange coefficient $\alpha$ and the effective density $\rho^*_\beta$ such as:

$$\boldsymbol{D}^*_{A\beta} = D_{A\beta} \left( \boldsymbol{I} + \varepsilon_\beta^{-1} \frac{1}{V} \int_{A_{\beta\sigma}} \left( \boldsymbol{n}_{\beta\sigma} \boldsymbol{b}_\beta \right) dA \right) - \varepsilon_\beta^{-1} \left\langle b_\beta \tilde{\boldsymbol{v}}_\beta \right\rangle \tag{22}$$

$$\alpha = \frac{1}{V} \int_{A_{\beta\sigma}} \frac{\rho_\beta}{\left( 1 - \omega_{eq} \right)} D_{A\beta} \left( \boldsymbol{n}_{\beta\sigma} \cdot \nabla s_\beta \right) dA \tag{23}$$

$$\rho^*_\beta = \frac{1}{\varepsilon_\beta \ \Omega_{A\beta}} \left\langle \rho_\beta \omega_{A\beta} \right\rangle \tag{24}$$

Based on microscopic considerations and some assumptions described above, we finally get the macroscopic transport equation. The term involving the exchange coefficient $\alpha$ comes into the equation as a source term for the phase $\beta$ .We observed that when the saturation at a material point is reached then:

$$\omega_{eq} = \Omega_{A\beta}$$

$$\Rightarrow \frac{\partial \varepsilon_\beta}{\partial t} = 0 \Leftrightarrow \varepsilon_\beta = Cte$$

In the case of DIM use, i.e., not a real porous medium problem application, the choice of the exchange coefficient $\alpha$ expression as a function of porosity is more arbitrary. It must, however, be observed a null condition when the material point is considered strictly in the fluid phase or strictly in the solid phase. This is illustrated in Figure 7.

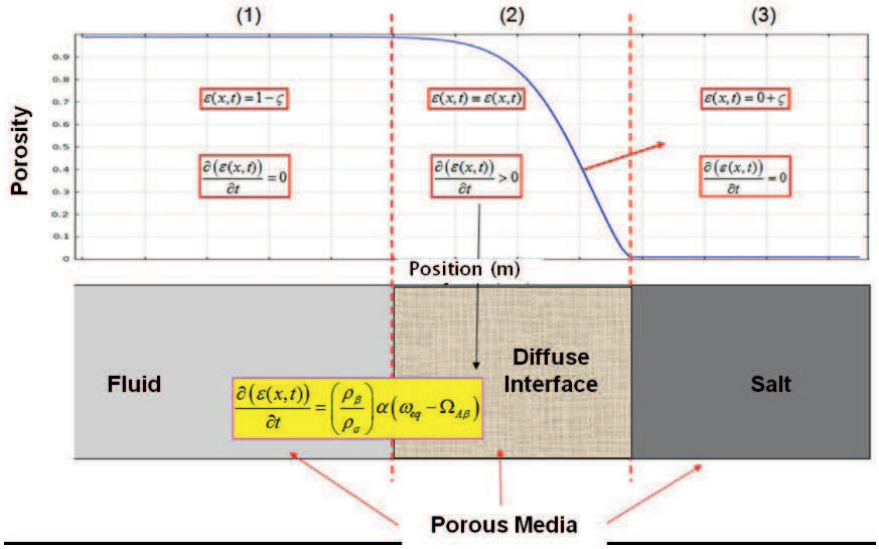


Figure 7: Porous domains: “fluid”-interface-solid and expression of volume fraction $\varepsilon$ .

We must underline that, in the DIM model, there is no “pure liquid phase” (Figure 7) since $\varepsilon_\beta$ is used continuously to represent the fluid as well as the solid regions. Therefore, the Navier-Stokes equations are no longer suitable for this situation. Instead, we can adopt a Darcy-Brinkman model (Brinkman 1947) to take the place of Navier-Stokes equations for the momentum balance equations

$$\frac{\mu_\beta\left(\Omega_{A\beta}\right)}{\varepsilon_\beta}\Delta \boldsymbol{V}_\beta - \left(\nabla P_\beta - \rho_\beta^* \boldsymbol{g}\right) - \mu_\beta\left(\Omega_{A\beta}\right)\boldsymbol{K}^{-1}\cdot\boldsymbol{V}_\beta = 0 \qquad (25)$$

where the permeability tensor ***K*** is a function of $\varepsilon_\beta$ . The Darcy-Brinkman equation will approach Stokes equation when ***K*** is very large and will simplifies to Darcy’s law when ***K*** is very small. If inertia terms are not negligible, a similar Darcy penalization of Navier-Stokes equations may be used. The resulting DIM equations may be solved with various numerical techniques but in this paper, we will use a COMSOL® implementation. Results are presented and discussed in the next section.

## 3 Numerical modelling

Whenever density variation is present in the fluid phases, the gravity (buoyancy force) can play a key role in mass and heat transports, through the mechanism of natural convection.

In our case, the dissolution of the salt walls results in higher concentrations around the interface than in other fluid regions. Therefore, it makes sense to study the influence of gravity effects upon the dissolution and fluid flow. To characterize the gravity effects for dissolution problem, one can refer to the Rayleigh number, Ra, which is defined as the ratio of buoyancy forces to mass and momentum diffusivities as

$$Ra = \frac{\Delta\rho_{max} |g| K_{max} L}{\mu_\beta D_\beta} \tag{26}$$

This natural convection phenomenon, often called salt fingering, is well illustrated by Figure 8 (Luo et al. 2015) (flow from left to right).

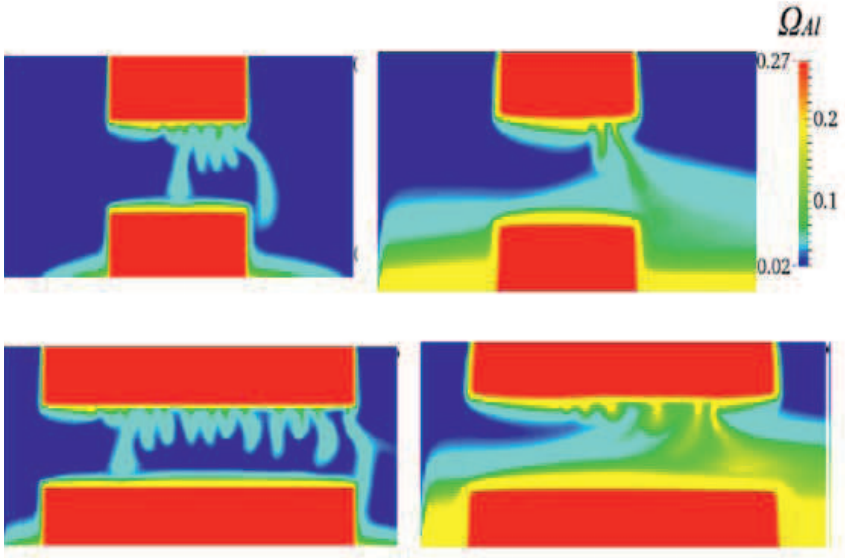


Figure 8: Examples of concentration plumes for a 2D simulation with gravity at time 100 s and 1000 s and salt block size 8 mm (top) and 16 mm (bottom), (*After Luo et al. 2015*).

We observe that the shape on the top of the channel loses its regularity and the onset of a wavy shape (roughness) is due to the coupling between dissolution and physical Rayleigh convective instability which induces a vortex motion of fluid particles. The heavy fluid (more saturated) goes downward and increases the dissolution upward. The potential occurrence of a coupling between dissolution and convective pattern may have a major influence when modeling the dissolution of cavities, as will be illustrated below.

### 3.1 Axisymmetric cavity

This section is devoted to the numerical modeling of an experimental “large scale” dissolution process. The goal is to show the ability of the DIM method to tackle difficult problems with geometry singularities and natural convection effects.

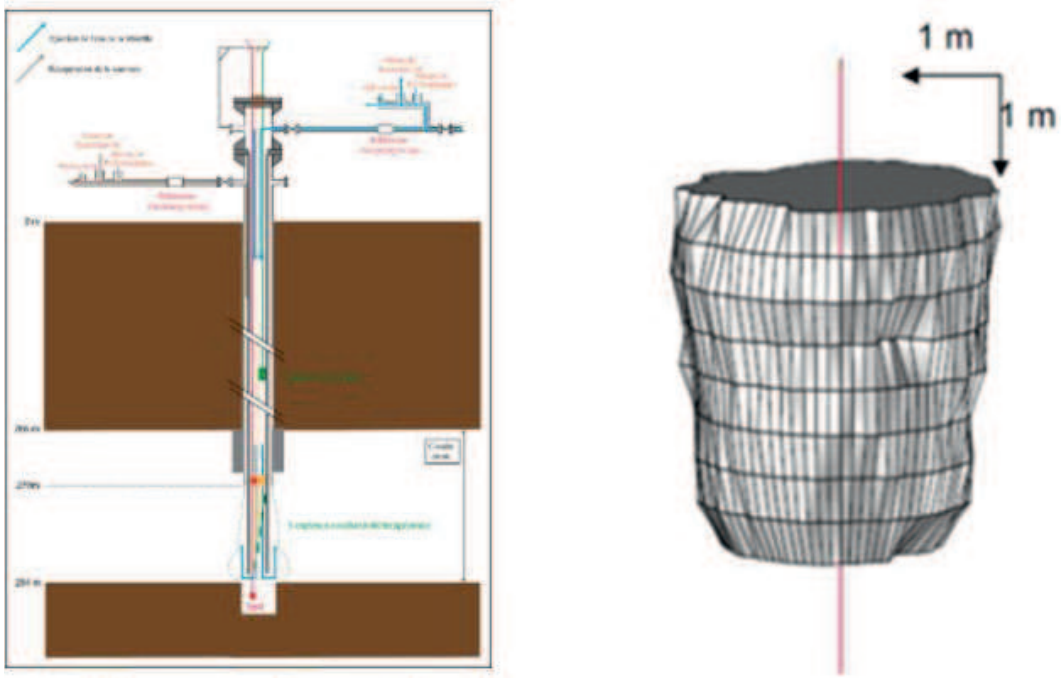


Figure 9: Illustration of the experimental salt rock dissolution process (right) and shape of the cavity after 12 days (right) (after Charmoille et al. 2012).

This test case is based on data coming from the Cerville pilot (Charmoille et al. 2012). We benefited from the availability of one of the salt exploitation surveys of the Cerville-Buissoncourt concession to carry out a dissolution experiment.

This concession belongs to Solvay which put its expertise and its operating logistics at the service of this experiment. The goal of this experiment is to obtain continuous in situ data on the formation process of dissolution cavities and to serve the numerical modeling testing and calibration.

The salt layer 6 m thick, is located at about 280 meters deep. It is limited in lower and upper parts by clay layers. A concentric leaching well (Figure 9) was drilled. The tubing is constituted of two concentric tubes.

Then fresh water was injected through the central tube during 12 days (Charmoille et al. 2012). This method is known as *direct leaching process*. The inlet flow is 3 $m^3$/h during 4 days followed by 1.5 $m^3$/h during 8 days.

The Figure 9 depicts the experimental setting and the final shape and size of the cavity (obtained by sonar).

We show Figures 11-15 some numerical results. Figure 10 shows the axisymmetric mesh and model.

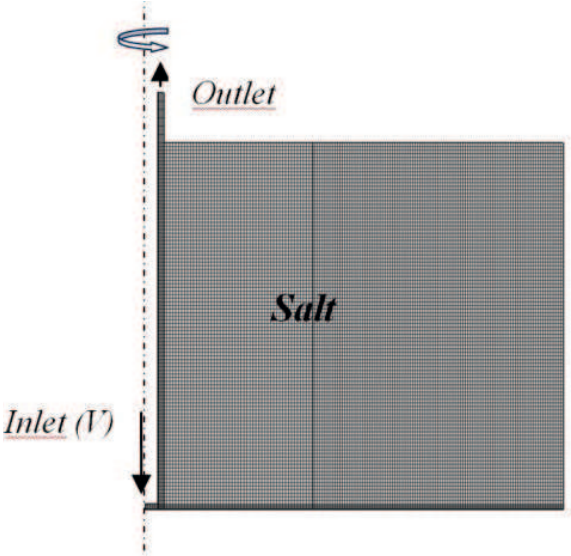


Figure 10: Geometry and boundary condition for the cavity dissolution model.

The imposed inlet velocity is 8 cm/s during 4 days and then 4 cm/s during 8 days.

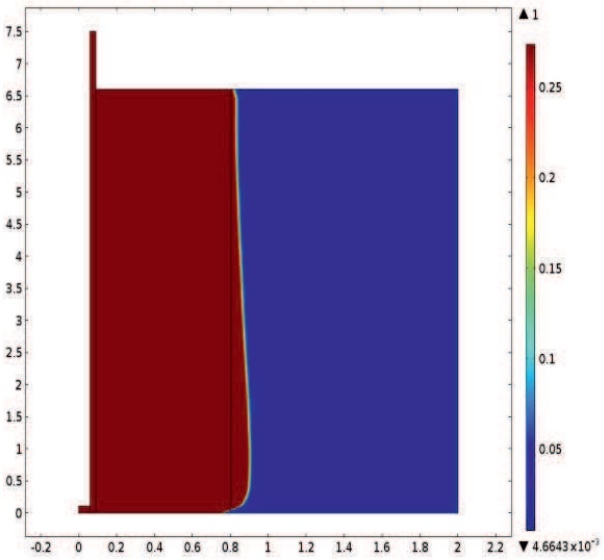


Figure 11: Isovalue of the porosity after 4 days. (void or pure fluid domain for unity).

From the axisymmetric shape of the cavity the computed dissolved volume is around 12 $m^3$, which is very close to the measured in-situ value around 11 $m^3$.

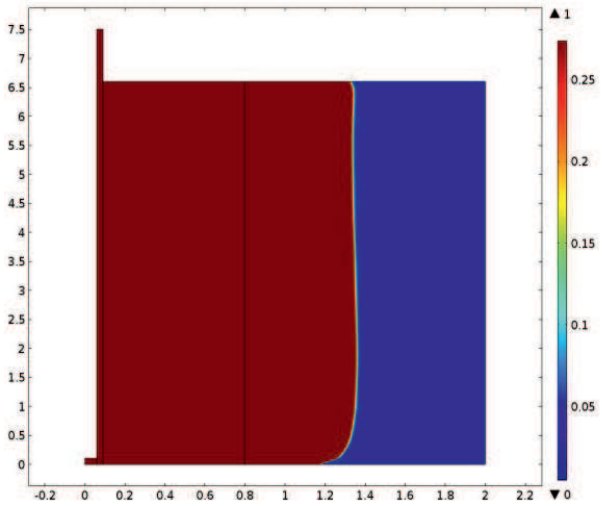

Figure 12: Isovalue of the porosity after 12 days (void for unity).

At 12 days (Figure 12), the computed dissolved volume is around 38 $m^3$ and the measured in-situ is around 40 $m^3$. Again a very good agreement given the fact that the formation was considered as homogeneous, which is seldom the case in natural media, and that the various uncertainties were not included in the model. Figure 13 represents the time evolution of *the diffuse* fluid-salt interfaces at various times (for a line located at the middle of the layer).

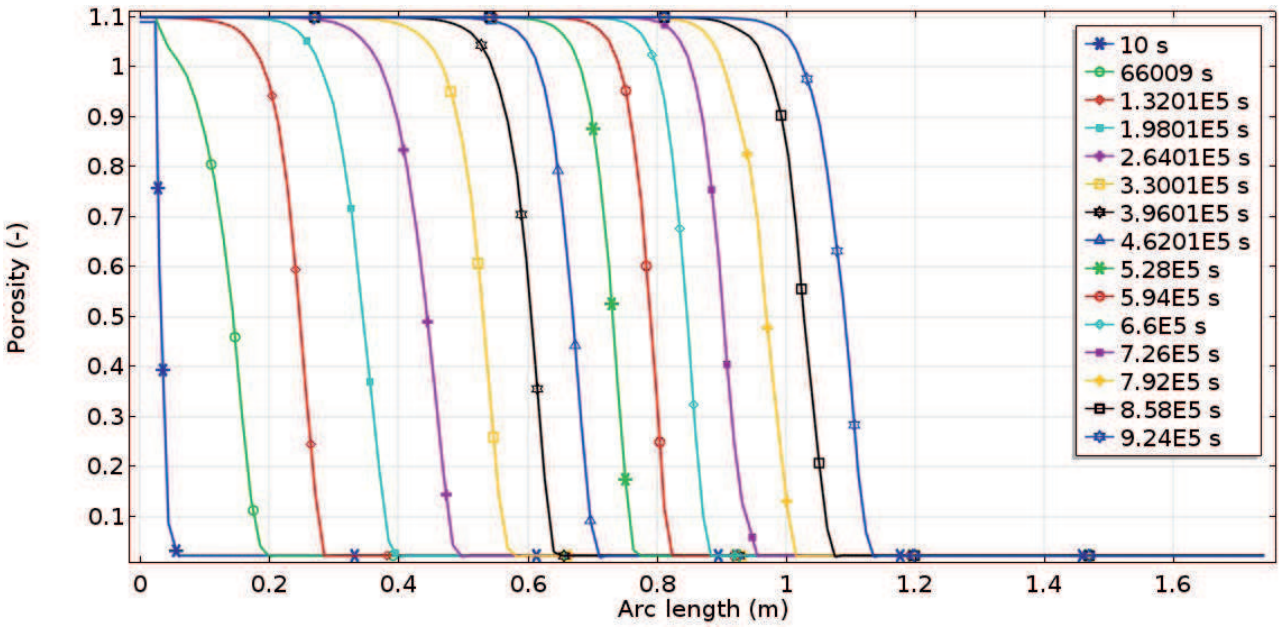


Figure 13: Examples of the distribution of the porosity at a line located at the middle of the model and at several times (1 to 12 days).

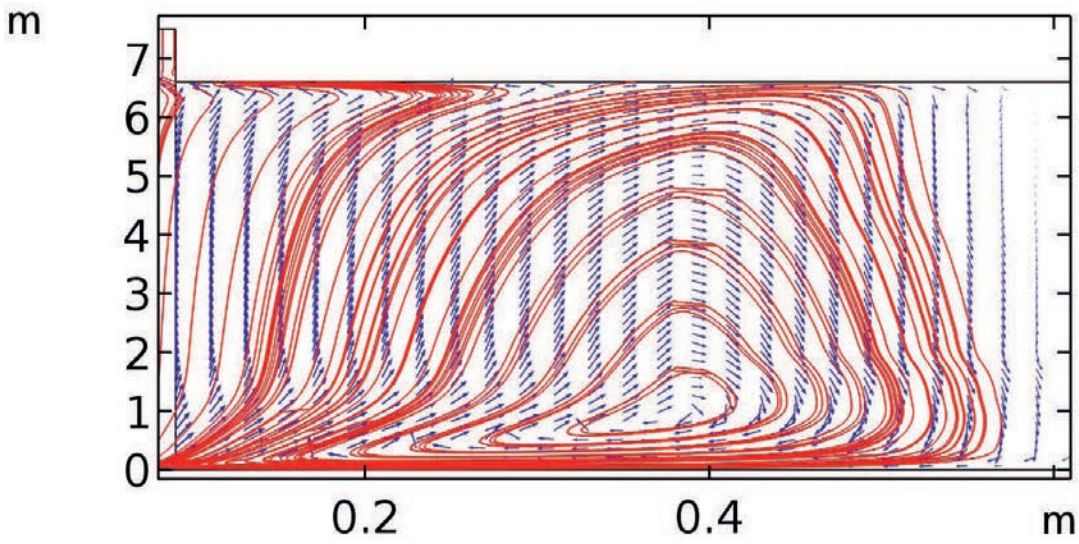


Figure 14: Streamlines and vectors field after 4 days

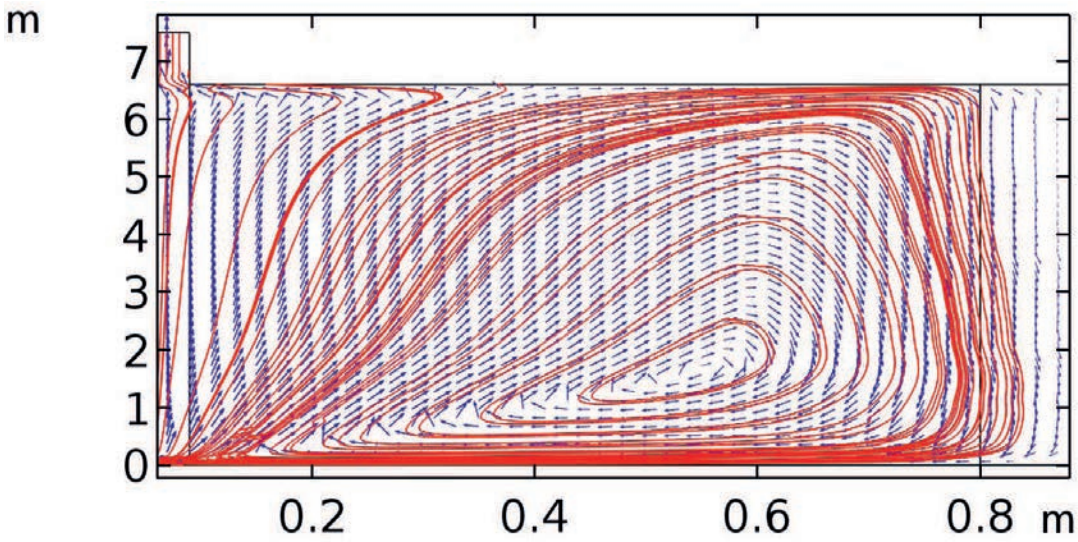


Figure 15: Streamlines and vectors field after 8 days

Figures 14 and 15 give illustrations of the complex streamlines and fluid velocity field at two time steps, illustrating the effect of natural convection. The numerical method was extended to a three-phases (gas-liquid-solid) problems (Luo et al. 2014) and to other dissolving matter. Gypsum, for instance, dissolves in flowing water about one hundred times more rapidly than limestone, but at only about one thousandth the rate of halite. Figures 16 show the shape of the cavity in a gypsum medium, using the same initial and boundary conditions of the salt problem dissolution.

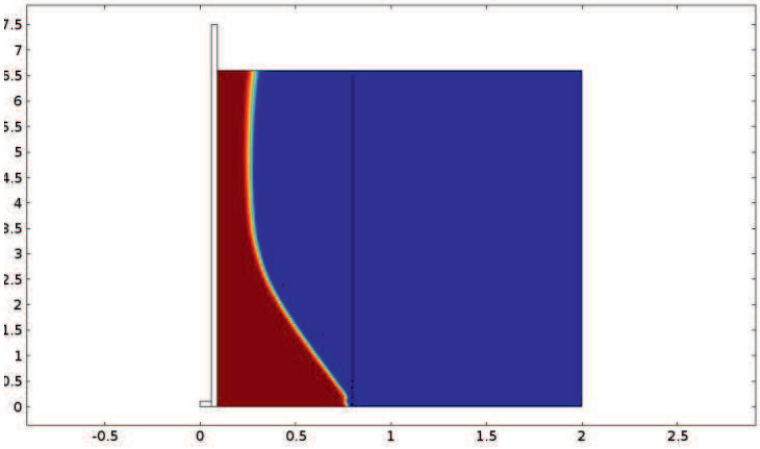


Figure 16: Isovalue of the porosity in gypsum after 10 years (void in red)

We observe the very low dissolution rate for gypsum material and a very different cavity shape due to the absence of natural convection because of the gypsum low solubility. Concentration in the case of salt dissolution is less monotonous due to the effect of mixed convection. After a given time, the dissolution or mass transfer from rock to salt is mainly driven by density gradients. While for gypsum, due to its small solubility, there is no natural convection and the rate of dissolution decreases smoothly as the front solid-liquid evolve with time.

## 4 Concluding remarks

For simulations of the solid-liquid dissolution process, one can use either explicit treatment methods (ALE for instance) or the presented diffuse interface methods (a local non-equilibrium DIM). The ALE is not suitable for simulating the problems with complex interfaces, e.g., sharp angles, porous media, as it relies strongly on the mesh shape. To the contrary, DIM is more practical to simulate dissolution problems, as the whole domain is used for solving through the introduction of a phase field (volume fraction of liquid phase in this paper). In this paper, following the idea from Golfier et al. (2002), a local non-equilibrium diffuse interface model based on a porous medium theory is extended to study dissolution problems with density variations taken into account.

As DIM considers the density variations, simulation with gravity becomes available. For a dissolution problem with high density gradients, for example, NaCl dissolved into water, Raleigh-Bénard physical instability can be aroused under this situation.

Instable flows, salt fingers, and interface wavelets are observed and impact locally the dissolution rate thus creating various interface structures with different shapes. These hydrodynamic instabilities are not only controlled by the Ra number but are also affected by forced convection and the Pe number (Luo et al. 2012). Forced convection may affect the concentration gradient as well as the dynamic of the salt fingering, which may be flushed out of the domain, thus changing the dissolution dynamics. This brings a strong source of flow complexity, as illustrated in the space Ra-Pe for a particular problem as discussed by Luo et

al. 2012. Such couplings between hydrodynamic instability and dissolution must be studied for each new initial boundary-value problem treated. Further, the potential advantage of using the diffuse interface model is that, since very fine meshes are required near the interface, it enables us to introduce automatic mesh refining algorithms, such as AMR (Luo et al. 2015) which can greatly improve the calculation speed.

Further works done in the field of cavity dissolution modeling will concern the mechanical behavior of the cavity structure. The deformation induced by the cavity formation will be taken into account. The coupling between pure dissolution processes and solid mechanics is necessary since the solid deformation will also influence the fluid flow. Although the interface motion due to the dissolution kinetics is several orders greater that those induced by salt creep, rock stress, etc., which should allow for a sequential approach to this problem.

## Acknowledgements

This study was funded through CORDIS an INERIS research program and J. Guo acknowledges the financial support of the Fundamental Research Funds for the Central Universities (grant number 2682016CX098).

## References

Anderson, D.M. & McFadden, G.B. 1998. Diffuse-interface methods in fluid mechanics. Annual Review of Fluid Mechanics, 30: 139-165.

Brinkman, H.C. 1947. A calculation of the viscous force exerted by a flowing fluid on a dense swarm of particles. Appl. Sci. Res., 1: 27-34.

Charmoille, A., Daupley, X. and Laouafa F. 2012. Analyse et modélisation de l'évolution spatio-temporelle des cavités de dissolution. Report DRS-12-127199-10107A. INERIS

Collins, J.B. & Levine, H. 1985. Diffuse interface model of diffusion-limited crystal growth. Phys. Rev. B, 31: 6119-6122.

Courtelieris, F. A., Delgado. 2012. Transport porocess in Porous Media. Springer

Donea, J., Giuliani, S. & Halleux, J.P. 1982. An arbitrary lagrangian-eulerian finite element method for transient dynamic fluid-structure interactions. Computer Methods in Applied Mechanics and Engineering, 33: 689-723.

Golfier, F., Zarcone, C., Bazin, B., Lenormand, R., Lasseux, D. & Quintard, M. 2002. On the ability of a darcy scale model to capture wormhole formation during the dissolution of a porous medium. Journal of Fluid Mechanics, 457: 213-254.

Guo, J., Quintard, M., Laouafa, F. 2015. Dispersion in Porous Media with Heterogeneous Nonlinear Reactions. Transport in Porous Media. Volume 109, Issue 3, pp 541-570.

Guo, J., Laouafa, F., Quintard, M. 2016. A theoretical and numerical framework for modeling gypsum cavity dissolution. Int. J. Numer. Anal. Meth. Geomech. 2016; 40: 1662- 1689. DOI: 10.1002/nag.2504.

Jeschke, A. A. and Dreybrodt, W. 2002. Dissolution rates of minerals and their relation to surface morphology. Geochimica et Cosmochimica Acta, 66, 3055-3062.

Jeschke, A. A., Vosbeck, K., Dreybrodt, W. 2001 Surface controlled dissolution rates of gypsum in aqueous solutions exhibit nonlinear dissolution kinetics. Geochimica et Cosmochimica Acta 2001; 65(1): 27-34.

Luo, H., Quintard, M. Debenest, G. & Laouafa, F. 2012. Properties of a diffuse interface model based on a porous medium theory for solid-liquid dissolution problems. Computational Geosciences, 16(4), 913-932.

Luo, H., Laouafa, F., Debenest, G., Quintard, M. 2015. Large scale cavity dissolution: From the physical problem to its numerical solution. European Journal of Mechanics B/ Fluids. Vol. 52, 131-146

Luo H., Laouafa F., Guo J., Quintard M. 2014. Numerical modeling of three-phase dissolution of underground cavities using a diffuse interface model. Int. J. Numer. Anal. Meth. Geomech.; 38: 1600-1616.

Quintard, M. and Whitaker, S. 1994. Transport in ordered and disordered porous media 1: The cellular average and the use of weighing functions. Transport in Porous Media, 14: 163-177.

Quintard, M. and Whitaker, S. 1994. Convection, dispersion, and interfacial transport of contaminant: Homogeneous porous media. Advances in Water Resources, 17: 221–239.

Quintard, M. and Whitaker, S. 1999. Dissolution of an immobile phase during flow in porous media. Ind. Eng. Chem. Res., 38: 833-844.

Taylor, R. and Krishna, R. 1993. Multicomponent Mass Transfer. Wiley-Interscience.

Whitaker, S. 1999. The Method of Volume Averaging. Kluwer Academic Publishers.